Annals of Materials Science & Engineering

Open Access

Austin Publishing Group

Research Article

Photocatalytic Activity of Sol-Gel Electrospun Co_3O_4 Nanofibers in Degrading Methylene Blue and Methyl Orange

George G and Anandhan S*
Department of Metallurgical and Materials Engineering, National Institute of Technology-Karnataka, India

***Corresponding author:** Anandhan Srinivasan, Department of Metallurgical and Materials Engineering, National Institute of Technology-Karnataka, Srinivas Nagar, Mangaluru-575025, India

Received: October 28, 2015; **Accepted:** December 20, 2015; **Published:** December 23, 2015

Abstract

In this work, Co_3O_4 ceramic oxide nanofibers were fabricated from sol-gel electrospun poly(styrene-*co*-acrylonitrile)/cobalt acetate tetrahydrate precursor composite fibers by calcination. The photocatalytic properties of Co_3O_4 nanofibers obtained at different calcination temperatures were studied using methylene blue and methyl orange as the model organic pollutants. The degradation of dyes occurred in the presence of an oxidative medium and the maximum degradation was observed for the fibers obtained at the lowest calcination temperature, which had a narrow band gap and smaller grains. The morphological and compositional features of the Co_3O_4 nanofibers obtained after calcination were studied by scanning electron microscopy and Fourier transform infrared spectroscopy. The results of X-ray diffraction study and Raman spectra revealed that the average grain size composing the fibers increased with the calcination temperature. A clear evidence of defects in the fibers was observed in ultraviolet-visible-near infrared (UV-Vis-NIR) and energy dispersive spectroscopic measurements.

Keywords: Electrospinning; Co_3O_4; Nanofiber; Photocatalysis

Introduction

Oxide nanomaterials have been widely used as photocatalysts for hydrogen evolution [1], methanol reduction, degradation of organic pollutants [2-6], antimicrobial activities [7], HCHO conversion [8] etc. ZnO, NiO, NbO, TiO_2 etc. and oxide nanomaterials doped with noble metals such as Ag, Au and Pt are some examples for such photocatalysts. The inertness or stability towards hazardous chemicals and high surface area of the metal oxide nanomaterials make them ideal materials for catalytic reactions. Most of the metal oxides are semiconducting in nature; therefore, the catalytic activity of these materials is triggered by excitation energy, which can excite the electrons from the valance band to the conduction band. These excited electrons act as initiators for the whole degradation process. Different regions of the visible-sun light are used as excitation energy, which are namely UV-A, UV-B, UV-C, visible white light and infrared. It has been proven that the nanofibrous oxides are strong candidates for solid state [9-11] and electrochemical sensing [12], where the catalyzed reaction between the target analytes and the oxide, and the electron transport are important. The high aspect ratio nanofibers are well suited for catalysis as well. Electrospinning assisted sol-gel processing is a widely accepted technique for the production of oxide nanofibers.

Many industrial effluents are carcinogenic and synthetic dyes are the most common among them. A wide range of physical, chemical and biological methods have been developed [13-15] for the purification of wastewater containing dyes. Chemical oxidation methods using chlorine, hydrogen and ozone as oxidants were widely employed for the purification purpose. However, the chemical method does not result in the complete neutralization of the organic pollutants [16]. Catalytic wet air oxidation and several other methods have been developed for removal of dissolved toxic organic pollutants from wastewaters; however, most of them failed due to either their inefficiency or due to an increased cost of treatment [17].

Heterogeneous catalytic reactions are successful in the complete oxidation of a variety of hazardous pollutants in waste water effectively and economically. A suitable selection of catalyst and reaction conditions can lead to a high selectivity towards environmentally harmful products under mild conditions. The presence of a good chemical oxidant in the medium can bring out non-catalytic chemical oxidation of the substrate in the bulk solution in addition to the heterogeneous catalytic processes taking place on the catalyst surface. Heterogeneous catalytic processes start by the adsorption of the organic pollutants on to the surface of the catalyst. As a whole, three simultaneous processes take place in a photocatalytic reaction, i.e., adsorption of organic dye on to the catalyst surface, excitation of catalyst and chemical oxidation of dye in the presence of chemical oxidant.

In this study, Co_3O_4 nanofibers were fabricated in three steps. In the first step, a spinnable sol of poly(styrene-*co*-acrylonitrile) (SAN)/ cobalt acetate tetrahydrate (CATH) was prepared. In the second step, the precursor composite fibers of SAN/CATH were fabricated through electrospinning process. These fibers were calcined above the degradation temperatures of SAN and CATH in the final step. Fine structural features are expected for the fabricated Co_3O_4 nanofibers as the interaction between the nitrile group of SAN and the carbonyl group of cobalt acetate can ensure the uniform mixing of metal salt in the polymer solution [18]. The firm styrene side groups of SAN can act as a truss to transform the morphology of SAN/CATH

Citation: George G and Anandhan S. Photocatalytic Activity of Sol-Gel Electrospun Co_3O_4 Nanofibers in Degrading Methylene Blue and Methyl Orange. Ann Materials Sci Eng. 2015; 2(2): 1025.

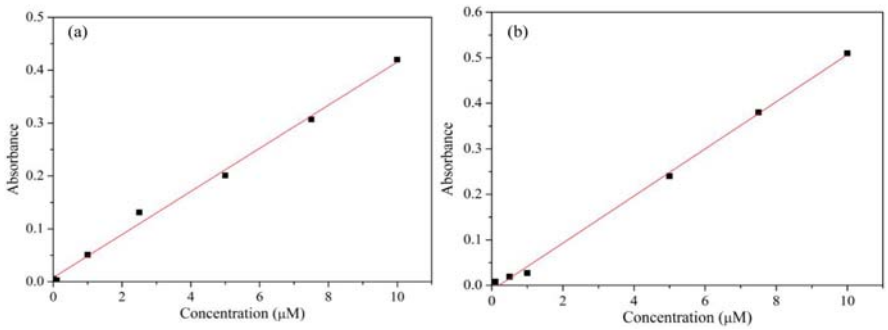

Figure 1: Calibration curves for (a) methylene blue (b) methyl orange.

composite fibers to Co_3O_4 nanofibers. The morphological and spectral characteristics of Co_3O_4 nanofibers were studied by different techniques. The photo-catalytic property of Co_3O_4 nanofibers were evaluated by investigating the degradation of two organic dyes, Methylene Blue (MB), a cationic dye, and Methyl Orange (MO), an anionic dye, in aqueous medium in the presence of hydrogen peroxide (H_2O_2) as a chemical oxidant under UV illumination.

Materials and Methods

SAN [Grade: Santron IMS 1000, acrylonitrile content: 30%, specific gravity: 1.07, $\overline{M}_v : 2.46\times10^6$ (viscometry), MFI: 35 g/10 min at 220°C under a load of 10 kg, ASTM D-1238] purchased from Bhansali Engineering Polymers, Rajasthan, India, cobalt (II) acetate tetrahydrate ($Co(OCOCH_3)_2.4H_2O$, assay 98%) (CATH) procured from High Purity Laboratory Chemicals, Mumbai, India and N, N-dimethylformamide (DMF) purchased from Sisco Research Laboratories Pvt. Ltd, Mumbai, India, were used without further purification to fabricate the precursor composite fibers. Hydrogen peroxide (H_2O_2) (molarity 34.1 g/mol) procured from Merck, Bangalore, India, methylene blue (MB) procured from Nice chemicals, Cochin, India and methyl orange (MO) purchased from BDH chemicals, Bombay, India were used for the degradation studies.

The precursor composite fibers were fabricated using electrospinning technique (E-Spin Nano, Physics Equipments Co., Chennai, India) using the sol containing 20 wt % SAN and CATH, respectively in DMF solution. The proportion by weight of SAN to CATH in the spinnable sol was 1:1 in this study. The optimal electrospinning conditions were determined, which correspond to minimum fiber diameter and a maximum yield. To do so, the applied voltage was varied as 15, 17, 20 and 22 kV, the tip to collector distance was 17 cm and the solution flow rate was 1000 μL h^{-1}.

The obtained SAN/CATH composite nanofibers were calcined in a programmable high temperature furnace (Indfur, Chennai, India) at a heating rate of 4 $K.min^{-1}$ and the calcination temperature was varied as 773, 873 and 973 K, the dwell period was 2 hours in all cases. The minimum calcination temperature was based on the degradation temperature of the SAN/CATH composite fibers during their thermogravimetric analysis (TGA) (EXSTAR 6000 TG/DTA 6300, Japan) in a nitrogen atmosphere at a heating rate of 10 K min^{-1}.

The morphological features of the fibers were examined by scanning electron microscope (SEM) (JEOL JSM-6380LA, Japan) and transmission electron microscope (TEM) (S-5500, Hitachi, Japan). The complete elimination of the organic phases were confirmed using Fourier transform infrared (FTIR) spectra (Jasco FTIR-4200, Japan), X-ray diffraction patterns (XRD) (JEOL X-ray diffractometer, DX-GE-2P, Japan) and Raman spectra (inVia, Renishaw, UK). The band gap energies were estimated using UV-Vis-NIR spectra (Varian, Cary 5000 UV-Vis-NIR, USA) of the ceramic fibers. The specific surface areas of the Co_3O_4 nanofibres were measured by the BET method (Smart sorb 92/93, Smart Instruments Co. Pvt. Ltd, Dombivli, India).

The photocatalytic activity of Co_3O_4 nanofibers on the degradation of MB and MO in the presence of UV light were carried out in a photocatalytic reactor chamber equipped with four 8 Watt UV lamps (Philips, 8W, TUV, UV-C). 50 mg of Co_3O_4 nanofibers were added to 100 mL solution of 80 mM H_2O_2 containing the dye (10 μM) in distilled water. Prior to UV illumination, the suspension was vigorously stirred by a magnetic stirrer in dark for 30 min to achieve an adsorption/desorption equilibrium, and the adsorption of the dye on the Co_3O_4 fibers was calculated. At specific time intervals, about 3 mL of the suspension were taken from the reaction chamber and analyzed with UV spectroscopy to study the degradation of the dye.

During UV exposure, stirring was maintained to keep the suspension homogenous. The concentration of dye in each degraded sample was determined using a UV spectrophotometer (Ocean optics USB-4000, USA) at a λ_{max} of 463 nm in the case of MO and 663 nm for MB. A calibration curve was obtained by plotting absorbance at λ_{max} *vs.* concentration (Figure 1). The percentage of degradation of MB and MO was obtained at different time intervals. The percentage photodegradation is given by equation 1.

$$y = \frac{C_o - C_t}{C_o} \times 100 \qquad (1)$$

Where C_o is the initial concentration and C_t is the concentration at time 't'.

Results and Discussion

Characterization of precursor composite fibers

Figure 2a shows the SEM image of the precursor fibers, obtained at an optimum spinning conditions (22 kV and 1000 μL.h^{-1}). The obtained SAN/CATH composite nanofibers are randomly oriented and uniform throughout its length. The TG plot of SAN/CATH composite fibers is shown in Figure 2b. SAN/CATH composite exhibits three step degradation. The onset of degradation for SAN is 663 K and the degradation ended at 773 K.

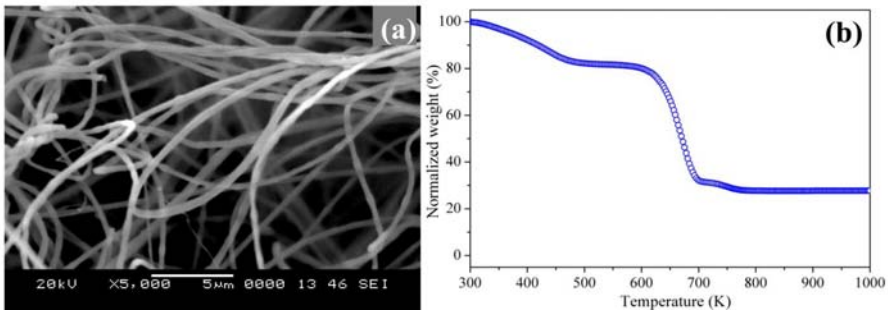

Figure 2: (a) SEM micrographs and (b) TG plot of SAN/CATH precursor fibers.

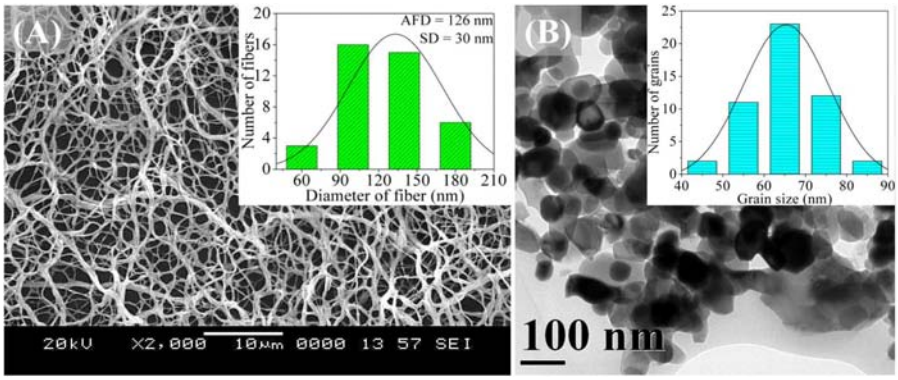

Figure 3: (a) SEM and (b) TEM images of Co_3O_4 nanofibers calcined at 773 K.

Characterization of cobalt oxide (Co_3O_4) nanofibers

Figure 3a shows the representative SEM images of random Co_3O_4 nanofibers obtained at a calcination temperature of 773 K and the corresponding diameter histograms. Due to the removal of SAN and acetate part of CATH, the sizes of the ceramic fibers are smaller than SAN/CATH composite fibers. TEM image of the grains composing Co_3O_4 nanofiber obtained at a calcination temperature of 773 K is shown in Figure 3b. The fibers are composed of a large number of equiaxial nanosized grains with well defined morphology.

Figure 4a shows the XRD pattern of the Co_3O_4 nanofibers obtained at 773 K and the standard JCPDS 65-3103 line diffraction pattern of Co_3O_4. The crystallographic peaks in XRD patterns correspond to Co_3O_4, since all the peaks exactly match with the standard peaks of Co_3O_4 as in Figure 4a.

The FTIR spectrum of Co_3O_4 nanofibers obtained at a calcination temperature of 773 K is shown in fig 4b. The peaks due to metal-oxygen covalent bond vibrations at 668 and 574 cm^{-1} confirm the formation of Co_3O_4 nanofibers. It is also noted that there are no peaks representing the organic groups as observed in the case of SAN/CATH, confirming the complete elimination of organic groups from the precursors.

The Raman spectrum of the Co_3O_4 nanofibers obtained at 773 K is shown in Figure 4c. For Co_3O_4 with spinel structure and O_h symmetry, the irreducible vibrational modes can be written as [1],

$$\Gamma = A_{1g} + E_g + 3F_{2g} + 5F_{1u} + 2A_{2u} + 2E_u + 2F_{2u} \qquad (2)$$

Among these modes, the A_{1g}, E_g and the three F_{2g} modes are Raman active and the corresponding peaks are 688, 479, 191, 520 and 616 cm^{-1}, respectively.

Diffuse reflectance UV-visible absorption spectrum of Co_3O_4 nanofibers obtained at 773 K is shown in Figure 4d. The absorbance peaks in UV-Vis-NIR spectrum of the Co_3O_4 nanofibers are attributed to the following transitions; the band at 1460 nm is attributed to crystal field $^4A_2(F) \rightarrow {}^4T_1(F)$ transitions in the Co_3O_4 structure. The peak at 1220 nm is assigned to an "intervalence" charge-transfer $Co^{2+} \rightarrow Co^{3+}$ representing an internal oxidation-reduction process. Absorptions at 657 nm and 2788 nm are referred to ligand-metal charge transfer events $O^{2-} \rightarrow Co^{3+}$ and $O^{2-} \rightarrow Co^{2+}$, respectively [19]. The band gap energy of the fibers was determined with the help of Tauc plot (Table 1).

Use of Co_3O_4 nanofibers for catalytic degradation of synthetic dyes

Adsorption of dyes: During the adsorption studies, the time required to achieve an adsorption/desorption equilibrium was found to be 30 minutes and the results of MB and MO adsorption on the surface of the catalyst is shown in Figure 5. The adsorption of MO on the Co_3O_4 fiber surface was less as compared with that of MB at the neutral pH. Initially, the adsorption of MB onto Co_3O_4 surface may be less, since MB is cationic and Co_3O_4 fibers are p-type semiconductors. Later, the adsorption level is increased because of the interaction of water with the catalyst surface. The interaction of water molecules with the catalytic surface will lead to the formation of a negative polarity (deprotonation) on the catalytic surface [55], according to the following equations (equation 3 and 4), where '*S*' represents the catalyst surface.

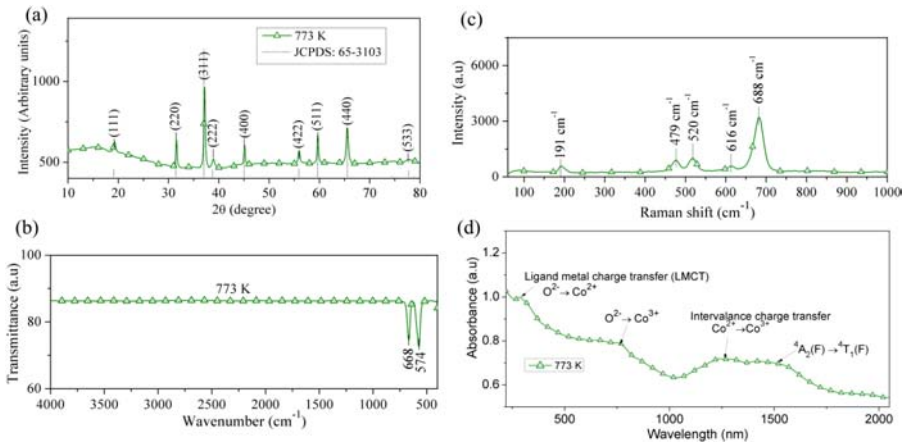

Figure 4: (a) X-ray diffraction pattern (b) FTIR spectrum (c) Raman spectrum and (d) UV-NIR spectrum of Co_3O_4 nanofibers obtained after calcination at 773 K.

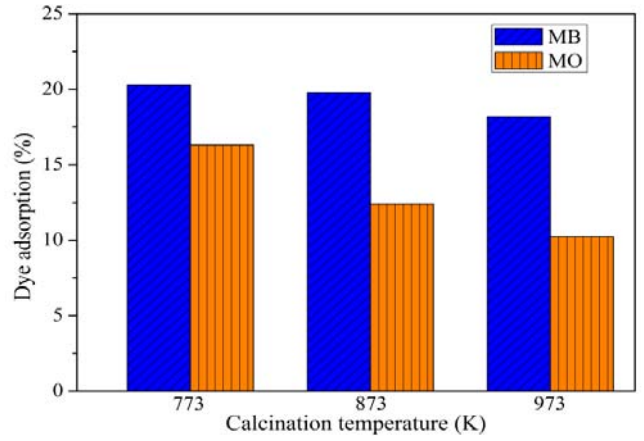

Figure 5: Adsorption of MB and MO on Co_3O_4 nanofibers obtained at different calcination temperatures.

$$S-OH+H_2O \rightarrow S-O^- + H_3O^+ \quad (3)$$

This reaction results in the increased adsorption of the cationic dye on the catalytic surface and the adsorption attains equilibrium after 30 minutes (equation 4).

$$S-O^- + MB^+ \rightarrow S-O^-MB^+ \quad (4)$$

Whereas, in the case of MO, anionic dye, the adsorption takes place immediately after the mixings of the catalyst and dye, before the interaction of water with the catalyst surface to form negative polarity, and the adsorption is not increased once the polarity of the catalyst surface is changed. It was also noted that as the calcination temperature of the Co_3O_4 fibers were increased, the adsorption of the dyes were decreasing, due to the decrease in surface area with calcination temperature as in Table 1.

Catalytic activity: Co_3O_4 is a semiconductor, which absorbs energy greater than or equal to its band gap energy during the photocatalysis. This absorption leads to the excitation of electrons from the valance band to the conduction band of the catalyst. Such charge separation leads to the formation of electron-hole pairs, which can further generate free radicals in the system for oxidation of the organic species. The resulting free-radicals such as hydroxyl (•OH) by the interaction of H_2O_2 or H_2O with catalyst are very efficient oxidizers of organic materials and can degrade pollutants as in the case of UV/H_2O_2 mechanism [13,17]. In the present study, hydrogen peroxide decomposition takes place only in the presence Co_3O_4 catalyst, since the UV radiation used in this investigation is not falling in the absorption range of H_2O_2.

It is also important to note that the formation of hydroxyl radical takes place during the oxidation as well as reduction process at the catalyst surface, which will enhance the degradation process tremendously. The mechanism of catalytic action is depicted in Figure 6.

In the presence of H_2O_2, the hydroxyl radicals are formed easily, since the radical formation from H_2O_2 needs less activation energy as compared with the radicalization of H_2O, O_2 or any other electron acceptor molecules [20]. H_2O_2 is readily radicalized by absorbing the electron from the conduction band of the catalyst preventing the recombination of electrons in the conduction band to the holes in the valance band (Figure 6) [21]. In other words, in Co_3O_4/H_2O_2/UV system, the radicalization of H_2O_2 takes place at a faster rate than the recombination process.

In the presence of excitation energy H_2O_2 itself can be degraded to form •OH radicals as in equation. 5.

$$HO-OH \xrightarrow{h} OH^{\bullet} + {}^{\bullet}OH \quad (5)$$

Table 1: AFD, composition, band gap energy and specific surface area of Co_3O_4 nanofibers.

Calcination temperature (K)	AFD (nm)	Atomic percentage (%)*		Band gap (eV)		Specific surface area (m^2/g)
		Oxygen	Cobalt			
773	126	36.56	63.44	1.4	2.72	15.65
873	101	41.59	58.41	1.4	2.83	7.16
973	95.9	43.09	56.91	1.35	2.85	6.86

*Theoretical atomic percentage of oxygen and cobalt in Co_3O_4 are 42.86 and 57.14 %, respectively

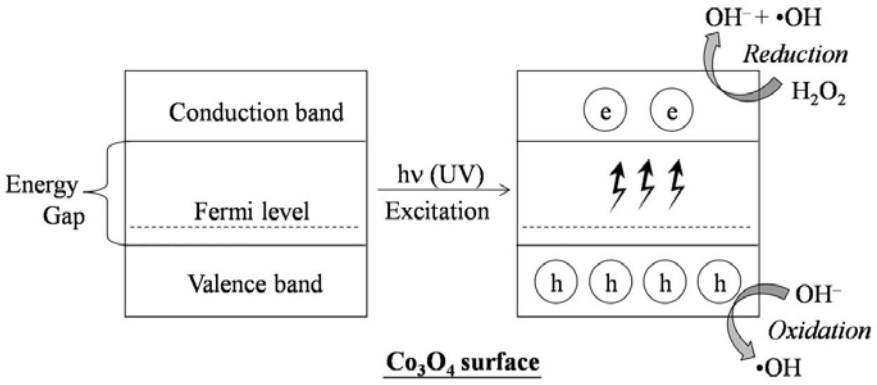

Figure 6: Mechanism of catalytic activity of Co_3O_4 surface in the presence of H_2O_2.

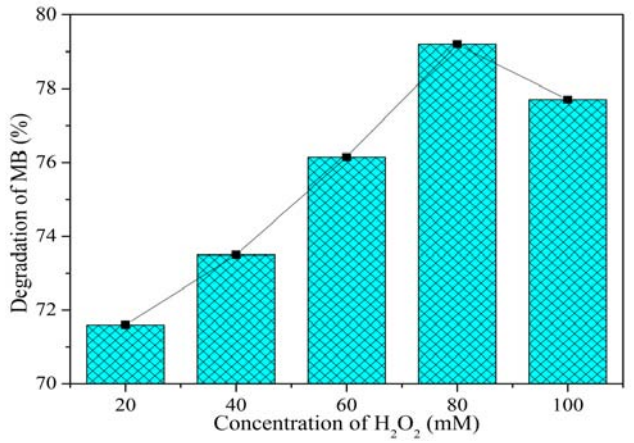

Figure 7: Optimization on the concentration of H_2O_2 for Co_3O_4 nanofibers obtained at 873 K.

The amount of H_2O_2 added for degradation study in the presence of Co_3O_4 was optimized as 80 mM (Figure 7). At low concentrations, H_2O_2 prevents the recombination of electrons, but, at higher concentrations H_2O_2 acts as an •OH scavenger (equation 6 & 7) [22] or it can be adsorbed to catalyst surfaces to reduce their catalytic activity [23].

$$H_2O_2 + OH^{\bullet} \rightarrow . HO_2^{\bullet} + H_2O \quad (6)$$

$$HO_2^{\bullet} + OH^{\bullet} \rightarrow H_2O + O_2 \quad (7)$$

Degradation of dyes: The photocatalytic activities of Co_3O_4 nanofibers prepared at different calcination temperatures in degrading MB and MO are shown in Figures 8 & 9, respectively. The fibers obtained at 773 K exhibit a better catalytic activity than the fibers obtained at higher calcination temperatures, since it has rich oxygen as observed in EDS results and UV spectral analysis. These fibers have low band gap energies than those obtained at higher calcination temperatures. The richness in oxygen above the stoichiometric ratio reduces the energy of the conduction band and increases the energy of valance band. The Co_3O_4 nanofibers obtained at the lowest calcination temperature possess smaller crystallite size, excess oxygen and a narrow band gap as compared with those obtained at higher calcination temperatures. The richness of oxygen in fibers calcined at 773 K can also reduce the speed of electron-hole recombination [24]. Considering such defects on the photocatalytic activity, the presence of defects enhances the photocatalysis since defects can act as scavengers of charges, electrons and holes in Co_3O_4, to reduce the recombination losses and also to provide active sites for the degradation reaction [25]. But, for the fibers with larger grains and less defects have less available surface for the electron-hole pair generation.

The percentage degradation of MB at specific intervals of time is shown in Figure 8a, and the corresponding UV spectra at each time interval are shown in Figure 8b. The intensity of the peak at 663 nm gradually decreases as the duration of UV exposure increases, which finally disappears after 60 minutes. The degradation of dyes in presence of Co_3O_4/UV system is far less than that of Co_3O_4/UV/H_2O_2 system and the results are not reported here. But, the degradation of MB in the presence of H_2O_2 alone for the duration used in the present study is appreciable and it is due to the splitting of H_2O_2 to •OH in the presence of UV light and the possible mechanism is depicted in the equation 5.

A similar degradation profile is observed also in the case of MO, but the complete degradation has not taken place in the case of MO (Figure 9a & 9b). The degradation of dyes is based on the breaking of unsaturated bonds in the presence of hydroxyl radicals and the formation of •OH is totally dependent on the texture of the catalytic Co_3O_4 nanofibers.

The study of dye degradation in the presence UV light and H_2O_2 with and without catalyst reveals that the reaction in equation 5 is inefficient for the complete degradation of MB and MO as shown in Figure 8a & Figure 9a, respectively.

The overall catalytic degradation processes (equation 4 and 5) of dyes are shown in Figure 10. Initially, the dyes attain an adsorption/desorption equilibrium on the catalyst surface. In the first stage, the dyes are degraded to species 'A' in the presence of •OH radicals, which are formed near the catalyst surface. In the second step, the species 'A' attains an adsorption/desorption equilibrium on the catalyst surface and will be degraded to another species, say 'B', in the presence of •OH radicals and the process continues till the formation of final degradation products, H_2O and CO_2.

$$\text{Dye} \xrightarrow{OH^{\bullet},h} \text{Degradation product}(s) + CO_2 + H_2O \quad (8)$$

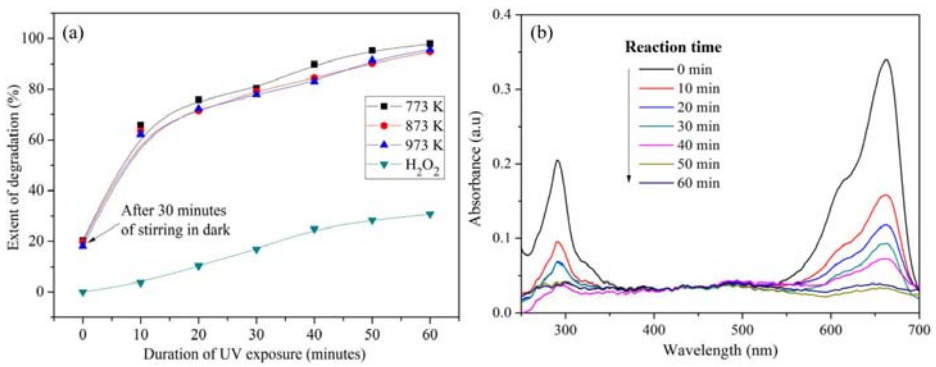

Figure 8: Degradation of MB (a) Percentage degradation with respect to time (b) corresponding UV spectra of Co_3O_4 nanofibers calcined at 873 K.

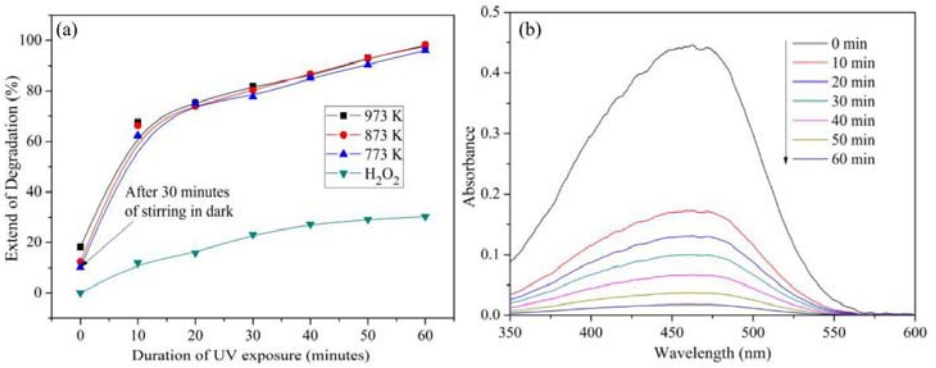

Figure 9: Degradation of MO (a) Percentage degradation with respect to time and (b) corresponding UV spectra of Co_3O_4 nanofibers calcined at 873 K.

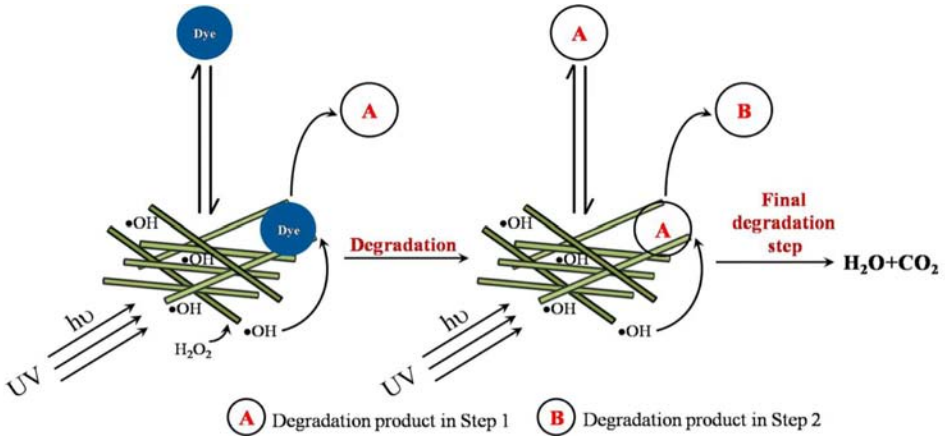

Figure 10: Mechanism of degradation.

Kinetics of photocatalysis: The kinetics of the photocatalytic degradation of dyes can be represented by first order equation [26],

$$h\left(\frac{C_o}{C_t}\right) = K_{app}t \qquad (9)$$

C_o is the initial dye concentration, C_t is the dye concentration after time t and K_{app} is the pseudo-first order rate constant.

Figure 11 shows the $ln(C_o/C_t)$ *vs.* duration of UV exposure in minutes for a fixed catalyst loading, in the presence of H_2O_2; also, the same is plotted for H_2O_2 in the absence of catalyst. All the degradation processes follow first order reaction kinetics, since the R^2 values of the linear fit is greater than 90. The first order rate constant and the corresponding R^2 values for the photocatalytic degradation of MB and MO are listed in Table 2. As the calcination temperature of the Co_3O_4 nanofibers is increased there is a reduction in the rate constant of the degradation reaction of both MB and MO. This reduction in the rate constant is attributed to the increase in the band gap as well as the increment in grain size as the calcination temperature is increased.

Degradation study using catalyst alone: In the presence of UV source a typical n-type photocatalyst shows direct catalytic degradation activity towards organic pollutants and can generate highly reactive

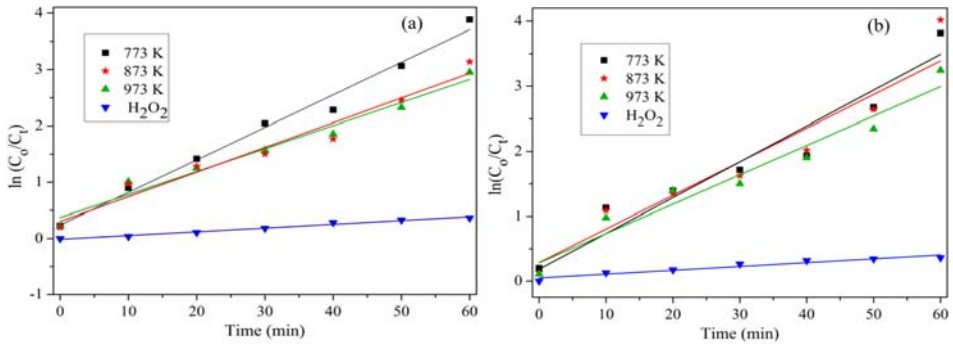

Figure 11: Kinetics of degradation of (a) MB and (b) MO.

Table 2: Rate constant for MB and MO degradation and the corresponding R^2 values.

Calcination temperature (K)	Methylene blue		Methyl orange	
	Rate constant (K_{app}) (min^{-1})	R^2	Rate constant (K_{app}) (min^{-1})	R^2
773 K	0.05645	98.5	0.05511	92.1
873 K	0.0438	96.8	0.0517	91.1
973 K	0.0408	95.4	0.04519	94.2
No fibers, H_2O_2 alone	0.00669	97.9	0.00593	91.9

hydroxyl radicals, since the number of available electrons are more in those systems as compared with the present Co_3O_4 nanofibers, which is a p-type material. The activity of Co_3O_4 nanofibers in degrading dyes depends either on the number electrons in the conduction band or the holes in the valence band. Degradation of dyes by Co_3O_4 nanofibers alone was not appreciable for the duration of UV exposure used in present study. It may be due to the immediate recombination of electron-hole pair formed during the UV excitation, which will not allow the formation of free radicals and the degradation commences only with the help of holes in the valance band of Co_3O_4.

The discoloration of MB happened after UV irradiation in the presence of catalyst alone, but, the blue color of the dispersion was restored when the irradiation was stopped and the system was exposed to atmospheric oxygen for a short time.

The chromophore in methylene blue readily accepts an electron (or loses a proton) and gets reduced to a colorless compound. This reaction is readily reversed by atmospheric oxygen or other oxidizing agents. Therefore, it is deduced that the solution was photobleached and photobleach is a reversible process. Photogenerated electrons from the catalyst reduce MB to produce the colorless leucomethylene blue species [27], which is readily oxidized to MB precursor by oxygen. During this study, using catalyst alone resulted in decolorization of MB and not the degradation, due to the reversible photobleaching process. In the case of MO, no such photobleaching phenomenon was observed, but, the degradation rate was very less for an hour, duration of UV illumination used in the present investigation.

Conclusion

In summary, photocatalytic Co_3O_4 nanofibers were successfully fabricated through a sol-gel combined electrospinning process. The SAN/CATH precursor composite fibers with the smallest average fiber diameter were obtained at an applied voltage of 22 kV, tip to collector distance of 17 cm, solution flow rate of 1000 $\mu L.h^{-1}$ and a solution concentration of 20 w/v %. The Co_3O_4 nanofiber diameters were reduced significantly after calcination, as compared with that of the SAN/CATH fibers. The complete elimination of organic phases from the precursor fibers were confirmed FTIR, Raman and XRD results. The presence of defects in these fibers made a difference in their band gap energies. The Co_3O_4 nanofibers were efficient in degrading the organic dyes methylene blue and methyl orange. The adsorption of dyes and rate constant of the dye degradation were dependent on grain size and band gap of the Co_3O_4 fibers.

Acknowledgement

G.G. would like to thank the dept. of Metallurgical and Materials Engg., National Institute of Technology of Karnataka (NITK), India for a research fellowship. The authors thank Ms. U. Rashmi and Ms. Akshata G. Patil for their kind assistance in scanning electron microscopy and X-ray diffraction, respectively. Authors would like to thank Dr. H. S. Nagaraja and his research student Mr. Sreejesh M. of department of Physics, and Mr. Liju Elias of department of Chemistry, National Institute of Technology of Karnataka (NITK), India, for their support for degradation studies. The authors also thank Dr. I. Regupathi department of Chemical engineering, National Institute of Technology of Karnataka (NITK) for availing the TGA facility. CIF, Pondicherry University, India is acknowledged for its kind assistance in Raman spectroscopy of the samples. The authors are very grateful STIC, Cochin, India, for the UV-NIR analysis of the samples and AVANSA technologies, Kanpur for the TEM analysis of the samples.

References

1. Korzhak AV, Ermokhina NI, Stroyuk AL, Bukhtiyarov VK, Raevskaya AE, Litvin VI, et al. Photocatalytic Hydrogen Evolution over Mesoporous TiO_2/metal Nanocomposites. J Photochem Photobiol A. 2008; 198: 126–134.

2. Rekha K, Nirmala M, Nair MG, Anukaliani A. Structural, Optical, Photocatalytic and Antibacterial Activity of Zinc Oxide and Manganese Doped Zinc Oxide Nanoparticles. Physica B. 2010; 405: 3180–3185.

3. Umadevi M, Jegatha Christy A. Synthesis, characterization and photocatalytic activity of CuO nanoflowers. Spectrochim Acta A Mol Biomol Spectrosc. 2013; 109: 133-137.

4. He H, Yang S, Yu K, Ju Y, Sun C, Wang L. Microwave induced catalytic degradation of crystal violet in nano-nickel dioxide suspensions. J Hazard Mater. 2010; 173: 393-400.

5. Warang T, Patel N, Fernandes R, Bazzanella N, Miotello A. Co_3O_4 Nanoparticles Assembled Coatings Synthesized by Different Techniques for Photo-Degradation of Methylene Blue Dye. Appl Catal B. 2013; 132–133: 204–211.

6. Vinodgopal K, Kamat PV. Enhanced Rates of Photocatalytic Degradation of an Azo Dye Using SnO_2/TiO_2 Coupled Semiconductor Thin Films. Environ Sci Technol. 1995; 29: 841-845.

7. Foster HA, Ditta IB, Varghese S, Steele A. Photocatalytic disinfection using titanium dioxide: spectrum and mechanism of antimicrobial activity. Appl Microbiol Biotechnol. 2011; 90: 1847-1868.

8. Lv L, Su Y, Liu X, Zheng H, Wang X. Synthesis of Cellular-like Co_3O_4 Nanocrystals with Controlled Structural, Electronic and Catalytic Properties. J Alloys Compd. 2013; 553: 163–166.

9. Jiao F, Frei H. Nanostructured cobalt oxide clusters in mesoporous silica as efficient oxygen-evolving catalysts. Angew Chem Int Ed Engl. 2009; 48: 1841-1844.

10. Lu X, Huang X, Xie S, Zhai T, Wang C, Zhang P, et al. Controllable Synthesis of Porous Nickel–cobalt Oxide Nanosheets for Supercapacitors. J Mater Chem. 2012; 22: 13357–13364.

11. Hu G, Tang C, Li C, Li H, Wang Y, Gong H. The Sol-Gel-Derived Nickel-Cobalt Oxides with High Supercapacitor Performances. J Electrochem Soc. 2011; 158: A695–A699.

12. Yoon J-W, Choi J-K, Lee J-H. Design of a Highly Sensitive and Selective C_2H_5OH Sensor Using P-Type Co_3O_4 Nanofibers. Sens Actuators B. 2012; 161: 570–577.

13. Lin SH. Adsorption of Disperse Dye by Powdered Activated Carbon. J Chem Technol Biotechnol. 1993; 57: 387–391.

14. Zollinger H. Color Chemistry: Synthesis, Properties and Applications of Organic Dyes and Pigments. 2nd edtn. Weinheim, Germany: Wiley VCH. 1991.

15. El Qada EN, Allen SJ, Walker GM. Adsorption of Basic Dyes from Aqueous Solution onto Activated Carbons. Chem Eng J. 2008; 135: 174–184.

16. Zhang J, Lee K-H, Cui L, Jeong T. Degradation of Methylene Blue in Aqueous Solution by Ozone-Based Processes. J Ind Eng Chem. 2009; 15: 185–189.

17. Zhuo Q, Ma H, Wang B, Fan F. Degradation of methylene blue: optimization of operating condition through a statistical technique and environmental estimate of the treated wastewater. J Hazard Mater. 2008; 153: 44-51.

18. Pei CC, Leung WW-F. Enhanced Photocatalytic Activity of Electrospun TiO_2/ZnO Nanofibers with Optimal Anatase/rutile Ratio. Catal Commun. 2013; 37: 100–104.

19. Barreca D, Massignan C, Daolio S, Fabrizio M, Piccirillo C, Armelao L, Tondello E. Composition and Microstructure of Cobalt Oxide Thin Films Obtained from a Novel Cobalt(II) Precursor by Chemical Vapor Deposition. Chem Mater. 2001; 13: 588–593.

20. Lachheb H, Puzenat E, Houas A, Ksibi M, Elaloui E, Guillard C, et al. Photocatalytic Degradation of Various Types of Dyes (Alizarin S, Crocein Orange G, Methyl Red, Congo Red, Methylene Blue) in Water by UV-Irradiated Titania. Appl. Catal B. 2002; 39: 75–90.

21. Grätzel CK, Jirousek M, Grätzel M. Decomposition of Organophosphorus Compounds on Photoactivated TiO_2 Surfaces. J Mol Catal. 1990; 60: 375–387.

22. Sauer T, Cesconeto Neto G, José HJ, Moreira RFPM. Kinetics of Photocatalytic Degradation of Reactive Dyes in a TiO_2 Slurry Reactor. J Photochem Photobiol A. 2002; 149: 147–154.

23. Cater SR, Stefan MI, Bolton JR, Safarzadeh-Amiri A. UV/H_2O_2 Treatment of Methyl Tert-Butyl Ether in Contaminated Waters. Environ Sci Technol. 2000; 34: 659–662.

24. Justicia I, Ordejón P, Canto G, Mozos Jl, Fraxedas J, Battiston G, et al. Designed Self-Doped Titanium Oxide Thin Films for Efficient Visible-Light Photocatalysis. Adv Mater. 2002; 14: 1399–1402.

25. Wang J, Liu P, Fu X, Li Z, Han W, Wang X, et al. Relationship between oxygen defects and the photocatalytic property of ZnO nanocrystals in Nafion membranes. Langmuir. 2009; 25: 1218-1223.

26. Kaur J, Bansal S, Singhal S. Photocatalytic Degradation of Methyl Orange Using ZnO Nanopowders Synthesized via Thermal Decomposition of Oxalate Precursor Method. Physica B. 2013; 416: 33–38.

27. Galagan Y, Su W-F. Reversible photoreduction of methylene blue in acrylate media containing benzyl dimethyl ketal. Photochem Photobiol A. 2008; 195: 378–383.

Ann Materials Sci Eng - Volume 2 Issue 2 - 2015
ISSN : 2471-0245 | www.austinpublishinggroup.com

Citation: George G and Anandhan S. Photocatalytic Activity of Sol-Gel Electrospun Co_3O_4 Nanofibers in Degrading Methylene Blue and Methyl Orange. Ann Materials Sci Eng. 2015; 2(2): 1025.